Simulation activities for particle detectors R&D at Horizon-T and HorizonT-KZ cosmic rays experiments

by

Alisher

Duspayev

A Thesis Submitted to the Faculty of the

DEPARTMENT OF PHYSICS

In Partial Fulfillment of the Requirements

For the Degree of

BACHELOR OF SCIENCE

In the School of Science and Technology

NAZARBAYEV UNIVERSITY

2017

NAZARBAYEV UNIVERSITY SCHOOL OF SCIENCE AND TECHNOLOGY

As members of the Thesis Committee, we certify that we have read the thesis prepared by Alisher Duspayev entitled

SIMULATION ACTIVITIES FOR PARTICLE DETECTORS R&D AT HORIZON-T AND HORIZONT-KZ COSMIC RAYS EXPERIMENTS

and recommend that it be accepted as fulfilling the thesis requirement for the Degree of

Bachelor of Science.

Date: April 24, 2017

Dmitriy Beznosko

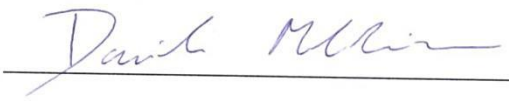

Date: April 24, 2017

Daniele Malafarina

Final approval and acceptance of this thesis is contingent upon the candidate's submission of the final copies of the thesis to the Department of Physics.

I hereby certify that I have read this thesis prepared under my direction and recommend that it be accepted as fulfilling the thesis requirement.

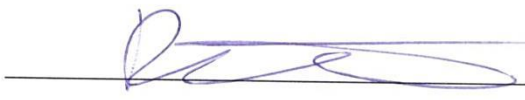

Date: April 24, 2017

Thesis Director: Dmitriy Beznosko

ABSTRACT

A nature of Ultra-high energy Cosmic Ray is one of the remaining open topics in the field of High Energy Physics. The modern detector systems are being designed and constructed to study this phenomenon. "Horizon-T" that is experiment located at Tien Shan high-altitude Science Station (TSHASS) near Almaty, Kazakhstan, is one of such systems, and there is work underway for a novel detector system "HorizonT-KZ" (HT-KZ). The HT-KZ is being developed by Nazarbayev University (NU) in collaboration with TSHASS and is planned to be installed here, at NU, Astana, Kazakhstan. A simulation of a single detector module that is aimed to determine the optimal detector arrangement and parameters is a significant part of the R&D process. A description and a discussion of the results of the simulation runs are presented in this thesis.

Table of Contents

List of Figures 1
List of Tables 2
1. Introduction 3
2. Extensive Air Showers 3
2.1. General information 3
2.2. EAS development 3
2.2.1. Hadronic part 3
2.2.2. Muonic part 4
2.2.3. Electromagnetic part 4
2.2.4. Cherenkov radiation 5
2.3. EAS Detection 5
3. Horizon-T experiment 6
4. HT-KZ experiment 7
5. Simulation Goals 9
6. Simulation description 9
6.1. Detector module description 9
6.2. General algorithm 9
6.2.1. Particle propagation and photon creation 9
6.2.2. Photon distribution and propagation in detection medium 10
6.2.3. Simulation of the side effects 10
6.2.4. Photon propagation in casing shell 11
6.2.5. Detection 12
6.3. Simulation of scintillator physics 12
6.4. Simulation of glass physics 12
7. Simulation validity check 13
7.1. x,y-coordinates 13
7.2. Zenith angle 15
7.3. Light yield isotropy 15
7.4. Light yield vs. zenith angle θ 17
7.5. Signal width vs. zenith angle θ 17
7.6. Uniformity vs. zenith angle θ 18

8. Glass detector simulation 20
8.1. Isotropy 20
8.2. Light yield vs. zenith angle θ 21
8.3. Signal width vs. zenith angle θ 21
8.4. Uniformity vs. zenith angle θ 22
8.5. Discussion 22
9. Comparison of 4 detector models 23
9.1. Light yield 23
9.2. Signal width 23
9.3. Uniformity 24
9.4. Discussion 24
10. Conclusion 24
11. Future plans for HT-KZ development 24
Bibliography 26

List of Figures

Figure 1: Feynman diagram of the charged pion most probable decay channel 4
Figure 2: Feynman diagram of the neutral pion most probable decay channel.....5
Figure 3: HT detector system from aerial view with 8 detection points labeled.....6
Figure 4: Scintillator detector at HT experiment [9] 7
Figure 5: Standard EAS signal at HT [9] 7
Figure 6: Example of "unusual" ("multimodal") event at HT [9] 8
Figure 7: Glass detector schematics: 3cm x 0.5m x0.5m glass base (in green), ~5cm diameter PMT above base at 0.5m (black disk), casing shell (in blue), and photon tracks (in red).....10
Figure 8: Distribution of initial *x*-coordinate of progenitor particles 15
Figure 9: Distribution of initial y-coordinate of progenitor particles 15
Figure 10: Distribution of initial zenith angle θ of progenitor particles.....15
Figure 11: Distribution of detected photons' progenitor particles' initial *x*,*y*-coordinates for scintillator detector with PMT above 16
Figure 12: Distribution of detected photons' progenitor particles' initial *x*,*y*-coordinates for scintillator detector with PMT below 16
Figure 13: Scintillator detector light yield vs progenitor particles' zenith angle.....17
Figure 14: Example of detected photons arrival time distribution 18
Figure 15: Scintillator signal width yield vs progenitor particles' zenith angle 18
Figure 16: Scintillator uniformity coefficient yield vs progenitor particles' zenith angle.....19
..Figure 17: Distribution of detected photons' progenitor particles' initial x,y-coordinates for glass detector with PMT above 20
Figure 18: Distribution of detected photons' progenitor particles' initial *x*,*y*-coordinates for glass detector with PMT below 20
Figure 19: Glass detector light yield vs progenitor particles' zenith angle.....21
Figure 20: Glass detector signal width vs progenitor particles' zenith angle 22
Figure 21: Glass detector uniformity coefficient vs progenitor particles' zenith angle.....22

List of Tables

Table 1: Parameters of 4 geometries obtained from the simulation.....**Error! Bookmark not defined.**

1. Introduction

Since the discovery of Higgs boson at CERN and neutrino oscillations at the Super-Kamiokande neutrino detector there are few open topics left in high energy physics (HEP). The study of cosmic rays, apart from the search for dark matter, is one of them. The origin and composition of Ultra-High Energy Cosmic Rays (UHECR) (typically defined at energies $>10^{18}$eV) is probably the most intriguing question in HEP. There are many theories on that, some name the active galactic nuclei as sources of UHECR [1], or even dark matter particle decay [2]. However, none of them has been confirmed experimentally so far. Another question concerned with UHECR is an absence of the anisotropy – e.g. no detectable direction to the source. Different models suggest several explanations for this phenomenon, but most of them appeal to the mentioned first question, the UHECR origin.

Studies of cosmic rays of such energies are possibly only by observing and analyzing the results of their interaction with the atmosphere - the Extensive Air Showers (EAS). A phenomenon of EAS has been studied in details since the middle of XX century; its brief overview follows below.

2. Extensive Air Showers[1]

2.1. General information

EAS is name for an extensive shower of particles born in hadronic and electromagnetic interactions in the atmosphere resulting from interactions between a primary particle from cosmic ray and air nuclei. This phenomenon was first observed by Bruno Rossi in 1930 [3], but it is widely accepted that the phenomenon was discovered by Pierre Auger [4] few years later. Energy of the primary cosmic ray varies in the enormous range of 10^9-10^{21}eV. The species composition of primary cosmic rays varies with the energy. Approximate composition of the primary cosmic ray with energy of 10^{15}eV: protons ~ 40%, α-particles ~ 20%, CNO nuclei ~ 20%, Al ~ 10%, Fe ~ 10%. In EAS, three main components are defined based on their interaction mode and range: hadronic, muonic and electromagnetic. All components together form a shower disk that can be up to few km in diameter. UHECR is a name for primary particles with the energies above 10^{18}eV or so; cosmic rays with such energies are assumed not to be originating from our galaxy [5], thus, they present a particular interest for HEP, astrophysics and cosmology.

2.2. EAS development

2.2.1. Hadronic part

The first interaction of the primary particle (e.g., proton p^+) occurs soon after it enters the atmosphere and interacts with a nucleon *A* typically belonging to nitrogen or oxygen nucleus. This reaction results in the pionization and ends with the creation of other nucleons *N* and a large number of charged ($\pi^{\pm}$) and neutral (π^0) pions, as well as a smaller number of protons, neutrons and other mezons, such as kaons and ρ-mezons:

[1] The content of this section in part is adopted from [23]

$$p^+ + A \rightarrow N + x * \pi^{\pm,0} + \cdots$$

Resulting energetic particles start interacting with other nuclei in a similar manner, thus a number of hadrons (from which pion is the lightest and most abundant hadron) multiplies.

2.2.2. Muonic part

When charged pions $\pi^{\pm}$ have energy <10^{11}eV or so, the probability to decay becomes larger than the probability of a hardonic interaction. This decay occurs via the most probable channel (branching factor of 0.999877 [6]) into a muon μ and muon neutrino ν_μ:

$$\pi^{\pm} \rightarrow \mu^{\pm} + \nu_\mu$$

This is a weak decay mediated by a W-boson between the two quarks that pion consists of; the Feynman diagram of the process is in Figure 1. Produced muons form the penetrating component of EAS disk that can reach up to 5km into the ground.

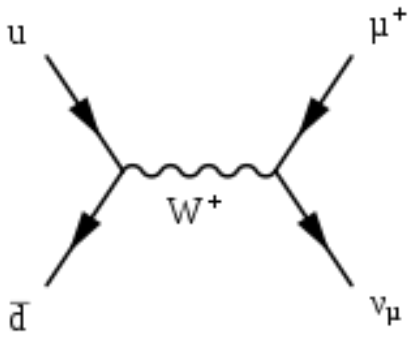

Figure 1: Feynman diagram of the charged pion most probable decay channel

2.2.3. Electromagnetic part

Neutral pion π^0 has the main decay mode (branching factor of 0.98823 [6]) of going to two photons γ, this is the electromagnetic interaction between up or down quark and its anti-quark (the diagram of this process is in Figure 2):

$$\pi^0 \rightarrow \gamma + \gamma$$

If energy of a single photon is >1.22 MeV (twice the rest mass of an electron), it may produce an electron-positron pair in the nucleus electric field with the probability increasing with the photon energy:

$$\gamma \rightarrow e^+ + e^-$$

However, if photon energy is above ~50KeV (but < 1.22Mev), it interacts exclusively via Compton scattering on electrons from air molecules and ionizing them. Produced electrons can undergo bremsstrahlung (breaking radiation) or Coulomb scattering on air atoms depending on its energy. Bremsstrahlung in air occurs mainly at electron energy >81MeV, whereas Coulomb scattering is dominant at the lower energies. Bremsstrahlung causes a high-energy photon emission that can produce another electron-positron pair. Positron eventually annihilates with

another electron, producing two gamma photons. These cyclic processes form the electromagnetic component of EAS.

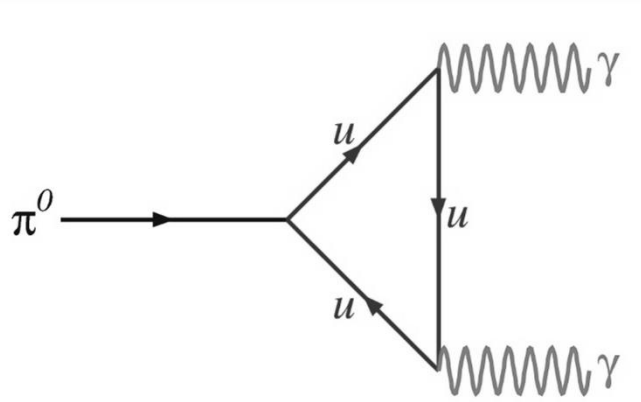

Figure 2: Feynman diagram of the neutral pion most probable decay channel

2.2.4. Cherenkov radiation

Multiple low energy photons can be emitted in the form of Cherenkov radiation (mainly from electrons with energy > 30MeV and muons). Typical EAS consists of millions of changed particles and produces a large amount of Cherenkov photons that also form a disk shape. Due to low refraction index of air (1.00028 at sea level), the angle between emitted photons and progenitor particle is very small (~1^0). The primary particle species, initial energy, EAS special and temporal particle density variation can be studied by detecting the components described.

2.3. EAS Detection

There are two main ground-based EAS detection methods: surface detector arrays (Cherenkov detectors and scintillator-based detectors) are used to detect secondary charged particles from EAS, optical telescopes (large mirrors and similar optical devices) detect fluorescence and Cherenkov radiation. Due to a large area of EAS disks, the detector systems occupy a large area as well (up to 3000km^2). Among the operating EAS detectors in the world its notable mentioning the latest ones: Pierre Auger Observatory in Mendoza Province, Argentina, Telescope Array Project in Utah, USA, the Tunka experiment (now named TAIGA) in Siberia, Russia, Ice-Cube in Antarctica and Horizon-T experiment (HT) [7] at Tien Shan mountains, Kazakhstan. HT is described in details in the next section, as the simulation works have been done for HorizonT-Kazakhstan (HT-KZ), system that will use the operating design concept of HT.

3. Horizon-T experiment

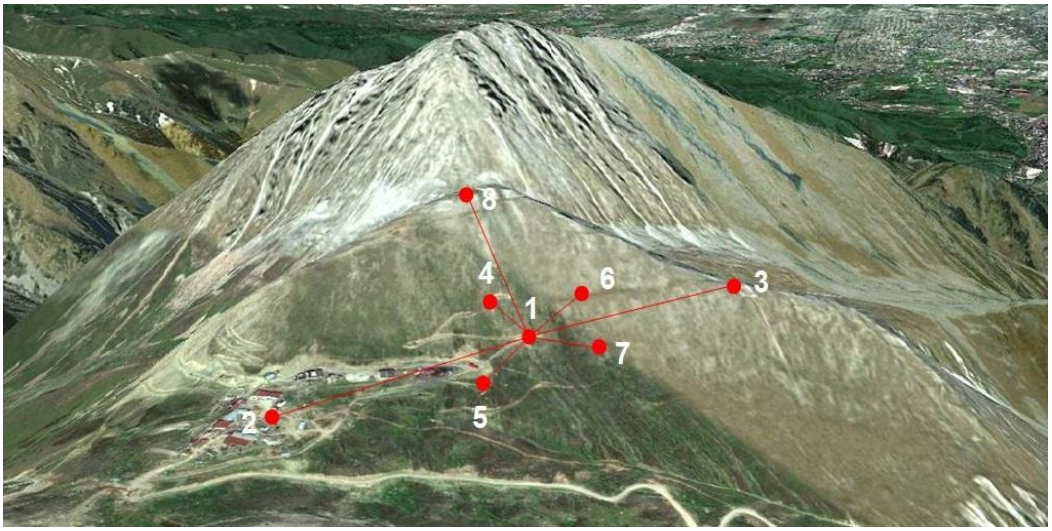

Figure 3: HT detector system from aerial view with 8 detection points labeled

HT is a detector system located at Tien Shan High-altitude Science Station (TSHASS) of Lebedev Physical Institute of the Russian Academy of Sciences at approximately 3340 meters above the sea level. It is constructed with the purpose to study EAS with initial energy $>10^{16}$eV and a wide zenith angle interval (0^0 - 85^0). HT consists of eight charged particles detection points and three Cherenkov light detectors that are used to detect Cherenkov light emitted by EAS charged components [8]. An aerial view photograph presenting a distribution of the system's detection points is in Figure 3. Note that the distance between detection points is up to 1km, such distribution allows to study EAS spatially as well as temporally [9].

HT obtains the angle coordinates of the incoming EAS using the chronotron method from the timing between detection signals at several points with the resolution better than 1 ns. The pulse time resolution of HT is <10ns. This value results as a minimum time resolution scale according to the CORSIKA [10] EAS simulation package that shows that the particles from vertically incoming EAS (~85^0 zenith angle) with ~10^{17}eV initial energy pass the observational level of HT in a few ns near the core and in ~15-20ns at 100m distance from the core. Current R&D works are aimed to improve the resolution scale of HT up to 2-3ns (currently ~7 ns).

Each detection point except point 8 has three scintillator detectors (SD) oriented perpendicularly to each other, point 8 has detector only in z direction (parallel to the sky). Such arrangement is implemented for the angular sensitivity in the detection process. Each scintillator has a square shape, its geometric sizes (1m base side, 5cm width) are used in the simulation described in this paper. A photograph of scintillator detector is in **Error! Reference source not found.**. Cherenkov detectors are located near point 1. Each detector consists of a 150cm diameter parabolic mirror with 65cm focal length. PMT is installed in the focal point of each mirror. A typical single EAS signal detected at all HT points is in Figure 4. Current R&D works are aimed to improve DAQ system as well.

Figure 4: Scintillator detector at HT experiment [9]

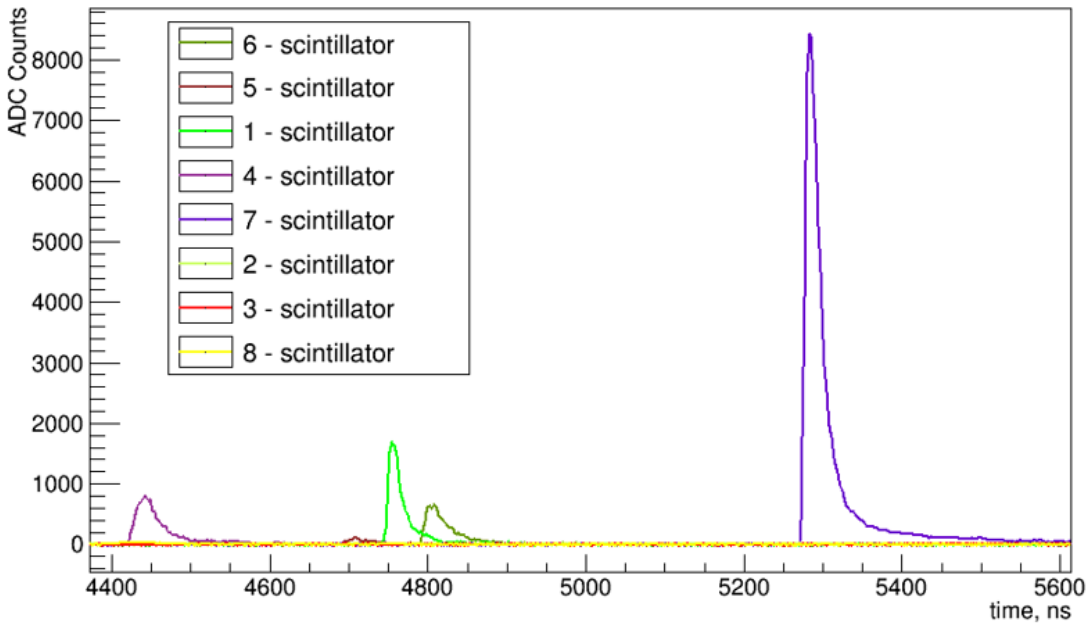

Figure 5: Standard EAS signal at HT [9]

The first construction plans for HT were proposed by R.U. Beisembaev in 1991 [11]. The first results were published in 2013 [12]. The last report about HT upgrades and performance is in [9]. As a part of collaboration with the personnel working at HT, a new detector system HT-KZ is being developed, it is considered in the next section.

4. HT-KZ experiment

HT-KZ is a distributed detector system under construction at NU, Astana, Kazakhstan. The main purpose of the system is to study the origin and the nature of Ultra-High Cosmic Rays (UHECR) with energies above ~10^{17}eV by analyzing EAS signals that arrive at the sea level. As it has been mentioned, HT-KZ construction is executed in collaboration with TSHASS, where HT, the predecessor to HT-KZ, operates currently. The first plans for HT-KZ construction are listed in [13], the last note on the HT-KZ design and construction progress is in [14]. HT-KZ is meant to further investigate properties of UHECR such as arrival anisotropy and multimodality of EAS originating from potential new particle type. The phenomenon of multimodal EAS is

being studied by the HT. It is attributed with the "unusual" detection signals, example of such a signal is in Figure 6 where multiple maxima (modes) in several channels are clearly visible (note difference with signal in Figure 4). The phenomenon was first observed by J. Jelly and W. Whitehouse in 1953 [15], but was considered at that time as an effect of particles' delayed arrival to the detectors. However, novel detector technologies and signal shape analysis indicate that an unknown phenomena may cause the "multimodal" events. Analysis of the signal shape presented in Figure 6 shows that it can be a result of multiple EAS disks arriving at large time differences. If it could be due to the delayed particles effect, a mass of the created particle should be much larger than of any known particle. In Standard model, probability for a particle to appear is proportional to $1/m^2$, so such events should have been very rare. HT shows that majority of high-energy events are, in fact, multi-modal Thus, this explanation is very unlikely. Main motivations for the HT-KZ construction is to study in detail findings from HT to find the multimodal EAS source(s) (a decay of the unknown heavy particle into several UHECR, existence of the exotic sources, e.g., dark matter particle decay).

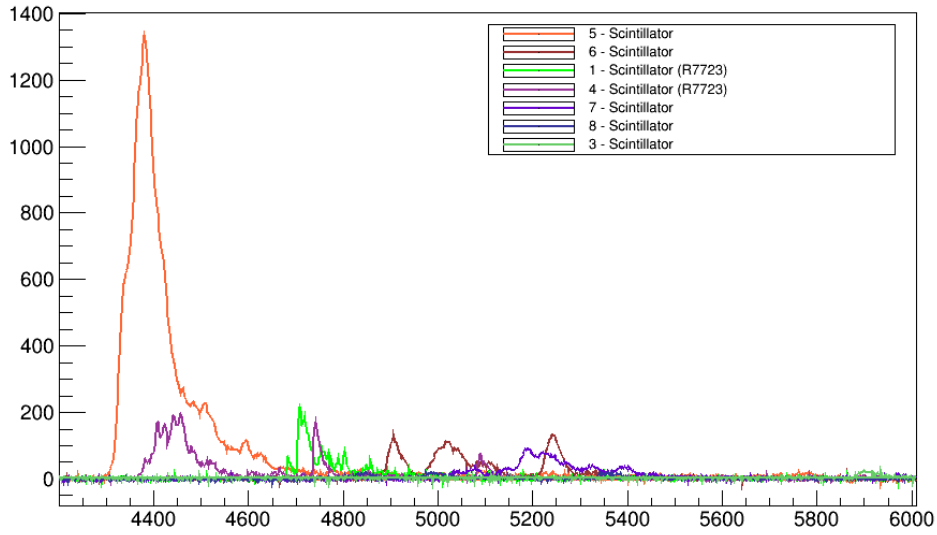

Figure 6: Example of "unusual" ("multimodal") event at HT [9]

The HT-KZ system will consist of at least ten modules to be distributed on the roofs of NU. Each independent module will consist of two plastic scintillator detectors for self-triggering. A possibility for liquid scintillator use is considered as well [16]. Each detector will consist of two parts: fast scintillator base (shape of the base has been chosen according to the recent simulation results [13]) and Hamamatsu [17] PMT (Photo Multiplier Tube). Each module will have expected time resolution ~1.5ns. About 1event/km^2 per day (~1000events/year) at primary particle energy of 10^{17}eV is expected with distance between modules ~150m. Each module is expected to collect data at rate <200kbyte/s.

Trigger level and logic of the system will be software controlled using CAEN [18] DT 5743 ADC. Contrary to HT that uses long cables that reduce pulse resolution, at HT-KZ the ADC is planned to be installed at each detection point. Data synchronization and analysis require the time resolution at ns level for better determination of the EAS structure and direction to the origin. Simulation of an individual module's operational process and measurements of the PMT linearity range have been completed [14]. Results of the simulation are presented in this work.

5. Simulation Goals

As it has been mentioned in the previous section, a design of a novel detector with fast response and wide detection range is necessary for an efficient performance of each detector module of HT-KZ system [14]. Several aspects must be considered before the actual construction of a single module. Simulation of the detector is needed to determine the following features:

- material to be used as a detection medium (scintillator, glass, etc.);
- PMT placement (above or below detection medium);
- outer casing shell that serves as a waveguide;
- painting the detector sides.

The very first simulation runs [13] showed that the air waveguide should be used between detection medium and PMT. Other parameters are checked using simulation results presented in the upcoming sections.

6. Simulation description

In this section, detector module implemented in simulation is described first, general algorithm of simulation code is explained, and then specific aspects of physics of different detector models are discussed.

6.1. Detector module description

In the simulation, the detection medium is a thin right parallelepiped with a thickness much smaller than side; PMT can be placed above or below detection medium at distance defined by user. Experimental observations indicated that the most efficient light detection is reached at the following arrangement: medium side opposite from PMT, its edges and the shell sides are painted (options are black or white), and PMT is placed above the unpainted side at the distance equal to the base side. In the text, the following convention is used: if PMT is placed above detection medium (e.g., glass), such geometry will be called "top-glass", if PMT is below detection medium (e.g., scintillator), we call this geometry "bottom-scint". The graphical representation of "top-glass" square simulated module is shown in Figure 7 with all elements represented by different colors.

6.2. General algorithm

6.2.1. Particle propagation and photon creation

At first stage, user enters a number of particles to use in the simulation run. Then, each particle is assigned random Cartesian *x*, *y*-coordinates across the detection medium surface, random polar angle φ in the interval [0; 2π] and zenith angle θ in the interval [0; $\frac{5\pi}{18}$] and a fixed *z*-coordinate. The interval for zenith angle is taken such that it corresponds to the experimental observations (detectors can register particles arriving with the angles within the specified interval of values). The particles direction is defined such that the particles travel from top to bottom of the detection medium. A number of emitted photons is calculated depending on the physics of the detection medium and particle path length and is determined at this step.

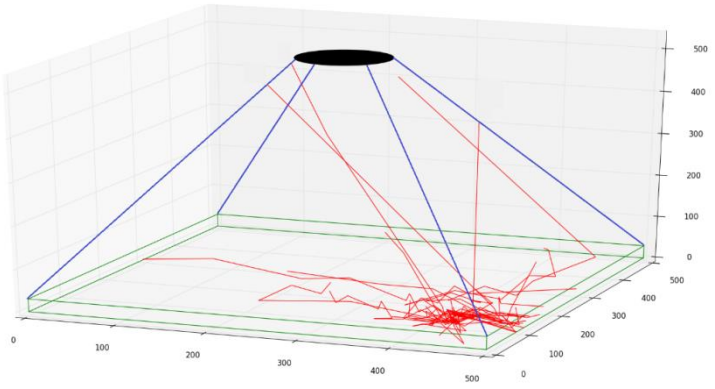

Figure 7: Glass detector schematics: 3cm x 0.5m x0.5m glass base (in green), ~5cm diameter PMT above base at 0.5m (black disk), casing shell (in blue), and photon tracks (in red)

6.2.2. Photon distribution and propagation in detection medium

All emitted photons are distributed along the path of progenitor particle using Poisson distribution (eq. 1):

$$p(k) = \frac{\lambda^k e^{-\lambda}}{k!} \quad (1)$$

where λ - number of emitted photons per propagation step (used as mean), k - number of emitted photons at particular point of the particle path. Using this process different number of photons is emitted at different points of the particle trajectory. Each photon is assigned the corresponding *x*, *y*, *z* - coordinates, a random polar angle φ_γ and a zenith angle θ_γ that can be random at some interval or a fixed value depending on the specific physics of the detection medium. In addition, initial time of a photon radiation is obtained using exponential distribution with characteristic time constant equal to the decay time of a particular medium. This is done to obtain expected shape of the signal from the simulated particle sample. The photons are propagated till they reach the medium boundaries.

6.2.3. Simulation of the side effects

Different processes can be observed depending on boundary between two media. Since the detection medium sides can be either painted or not, different physics is implemented in the simulation for each case.

6.2.3.1. Case of unpainted side

In this case simple laws of geometric optics that can be derived from classical electromagnetism are used. If a photon reaches an unpainted side, it can be reflected, refracted or absorbed by the medium. Which process will take place is chosen using Monte-Carlo (MC) processes [19], as well as critical angle reflection condition and corresponding probability values (e.g., probability of absorption). If an incident angle is less than the critical, photon can refract through the boundary (if not absorbed). Otherwise, it reflects back. Critical value is calculated using total internal reflection condition (Eq.2):

$$sin\alpha_c = \frac{n_{air}}{n_m} \quad (2)$$

where α_c - critical value of angle, n_m - detection medium refraction index, n_{air} - refraction index of the surrounding medium, which is air in our case (≈1).

If reflected, we use the fact (Eq. 3) that angle of reflection equal to the incidence one w.r.t normal:

$$\alpha_i = \alpha_{refl} \quad (3)$$

where α_i - photon's incident angle, α_{refl} - photon's angle after reflection. Which angle changes (polar, zenith or both) depends on the side, from which photon reflects, all possible cases are taken into account and verified by graphical representation of simulation results, thus, this aspect will not be discussed furthermore.

In a case of refraction, simple Snell's law (Eq. 4) is used:

$$n_m sin\alpha_i = n_{air} sin\alpha_{refr} \quad (4)$$

α_{refr}- photon's angle after refraction. If photon escapes the detection medium, whether it escapes at the side, where PMT is placed, is checked. If not, photon never reaches PMT and, thus, is not considered anymore (deleted from memory). Absorbed photons are treated in the same way. Note that in the implemented detection medium models photons can never refract through lateral sides, because they are always painted.

6.2.3.2. Case of painted side and diffusive reflection

In this case photons cannot refract through the sides (that is why PMT is always placed above the unpainted sides) and the diffusion reflection is used. Since the simulation is classical, a simple model of diffusive reflection is implemented [20]. After that, new polar and zenith angles of photon are calculated. MC sampling from cosine distribution (known as Lambert's cosine law, according to which, flux of the reflected light is proportional to the cosine of the angle between light direction and a normal to the plane of incidence) is used in this case:

$$sin\theta_{new} = \sqrt{\epsilon_1} \quad (5)$$

$$\varphi_{new} = 2\pi\epsilon_2 \quad (6)$$

In Eq. 5 and 6, $\epsilon_1 and\ \epsilon_2$ are random numbers from an interval [0;1].

6.2.4. Photon propagation in casing shell

As mentioned above, only those photons that escape detection medium from PMT side are considered further by the simulation algorithm. These photons are propagated till they reach the shell sides. As a photon comes to a side, its direction changes (if it is not absorbed): new polar angle is taken such that photon reflects inwards (does not refract), new zenith angle is calculated using diffusive reflection modeling described in the previous section. All "survived" photons are propagated till they reach the plane of PMT.

6.2.5. Detection

As a photon enters a PMT plane, whether it falls onto PMT region (implemented as a circle with 5.08cm/2 inch radius) is checked. If so, its detection possibility is checked using MC with 25% PMT efficiency. If the photon is detected, its initial coordinates (at what point of progenitor particle's trajectory it has been emitted) and total travel time are saved to corresponding output files. Total travel time is calculated as:

$$t_{total} = t_0 + \frac{d_m n_m}{c} + \frac{d_{out} n_{air}}{c} \quad (7)$$

where t_0 - initial time of a photon radiation, d_m - path traveled by photon in detection medium, d_{out} - photon path in the shell, $c \approx 3 * 10^8 m/s$ - speed of light.

6.3. Simulation of scintillator physics

The first material used as a detection medium in the simulation is a scintillator. It is a material that emits light due to an incident ionizing radiation. Due to the feature of scintillator to emit isotropic light the photons' zenith angles in this medium are taken randomly from the interval [0; π]. Thus, the photons' trajectory is obtained in a coordinate system of the detection medium. Optical rise time of a scintillator is taken as 4.5ns from the manufacturer specifications for a model of interest. A number of emitted photons per step (~560 photons/mm) is taken such that it corresponds to the previous experimental measurements of the scintillator light yield.

6.4. Simulation of glass physics

Another material used in simulation is thick optical glass. Relativistic charged particles emit only Cherenkov light while passing through this material. Cherenkov photons are emitted in a cone at fixed opening angle w.r.t. progenitor particle's trajectory. This angle is taken as a zenith angle of the photons in simulation and can be calculated as:

$$\theta = \cos^{-1} \frac{1}{n_m \beta} \quad (8)$$

where $\beta \approx 1$ - beta-factor of the parent particle which is ultra-relativistic. Due to anisotropy of the emitted light it is necessary to use a transformation from particle's coordinate system to medium's coordinate system. For that purpose the following transformation (Eq. 9) has been derived and used:

$$\begin{pmatrix} x'' \\ y'' \\ z'' \end{pmatrix} = \begin{pmatrix} \cos\theta\cos\varphi & \cos\theta\sin\varphi & \sin\theta \\ -\sin\varphi & \cos\varphi & 0 \\ -\sin\theta\cos\varphi & -\sin\theta\sin\varphi & \cos\theta \end{pmatrix} \begin{pmatrix} x \\ y \\ z \end{pmatrix} \quad (9)$$

where $\begin{pmatrix} x'' \\ y'' \\ z'' \end{pmatrix}$ - unit vectors in a particle's coordinate system, $\begin{pmatrix} x \\ y \\ z \end{pmatrix}$ - unit vectors in medium's coordinate system. Then, using:

$$\hat{r} = \begin{pmatrix} \sin\theta_\gamma\cos\varphi_\gamma & 0 & 0 \\ 0 & \sin\theta_\gamma\sin\varphi_\gamma & 0 \\ 0 & 0 & \cos\theta_\gamma \end{pmatrix} \begin{pmatrix} x'' \\ y'' \\ z'' \end{pmatrix} \quad (10)$$

and the trajectory of the photons in a medium coordinate system is obtained by substituting Eq. 9 into Eq. 10.

Optical rise time of glass is neglected as it is much smaller than the particle passage time through the glass volume (~100ps).

An emitted photons number per mm is calculated using standard Bethe-Bloch formula in a simplified form that is commonly used to estimate the photon number for the Cerenkov radiation in water and similar media (Eq. 11):

$$\frac{dN}{dx} = 2\pi\alpha\left(\frac{1}{\lambda_2} - \frac{1}{\lambda_1}\right)\left(1 - \frac{1}{\beta^2 n^2}\right) \quad (11)$$

where $\frac{dN}{dx}$ - number of photons per unit length, α - fine structure constant, λ_1, λ_2- wavelengths corresponding to the PMT detection range of ($\lambda_1 \approx 300nm, \lambda_2 \approx 500nm$), $\beta \approx 1$ - corresponding velocity of the incoming particles, $n \approx 1.6$ - glass refraction index. Although refraction index generally is a function of wavelength, this is not taken into account as the small differences don't impact the simulation outcome overall. According to Eq. 11, ~40 Cherenkov photons/mm are emitted in glass on average.

7. Simulation validity check

Scintillator detector model has been used to test the simulation validity by comparison with the experimental results from the existing modules. This model features square scintillator with 500mm base side, 30mm width as a detection medium. Lateral sides are painted black, bottom side is painted white. PMT is placed 500mm above the scintillator. Such model has been chosen for testing, since its parameters and features are known from detector calibration activities at HT experiment [21].

First, whether initial coordinates are distributed uniformly is checked, then dependence of 3 detector parameters on particle's initial zenith angle is examined: light yield, signal width and uniformity coefficient. To check these parameters an interval for progenitor particles' zenith angle is changed several times to determine the angle dependence. Isotropy of the scintillator detector is checked as well. According to the tests' results, which are presented below, simulation performs properly and can be used for further activities.

7.1. x,y-coordinates

First, it is necessary to check whether progenitor particles are assigned with uniformly distributed initial *x*,*y*-coordinates, that is, to check if there is no bias in implemented random number generators. Due to inconvenience to work with 2D-histrogram distributions of *x* (**Error!**

Reference source not found.) and *y* (

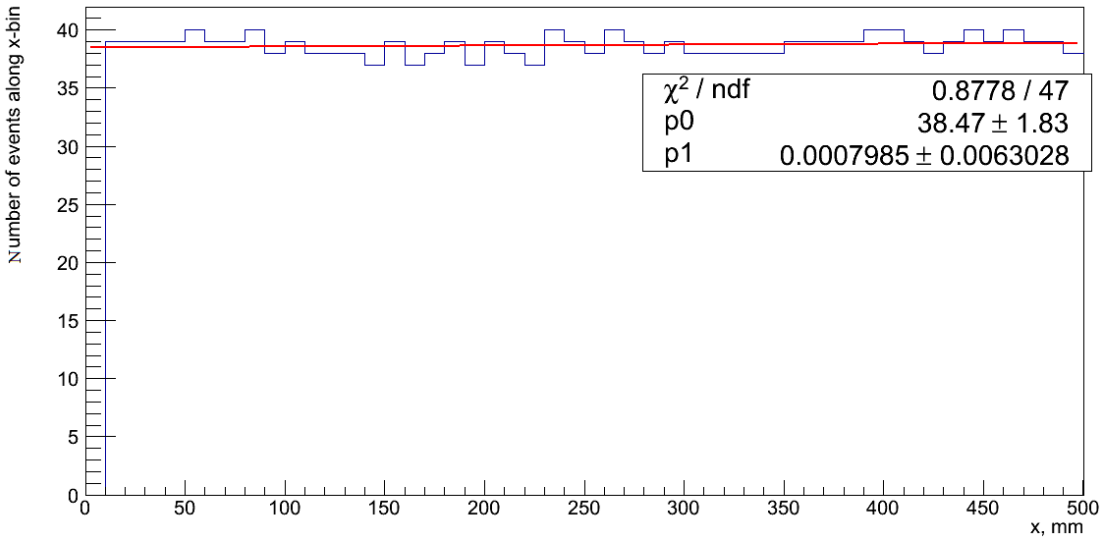

Figure 8: Distribution of initial *x-coordinate* of progenitor particles

Figure 9) coordinates are presented separately. Both 1D-histograms are fitted by linear function to check the slope. As it can be seen, the slopes are very small and on the same order as their errors, thus, we may conclude that the progenitor particles' initial Cartesian coordinates are distributed with adequate uniformity.

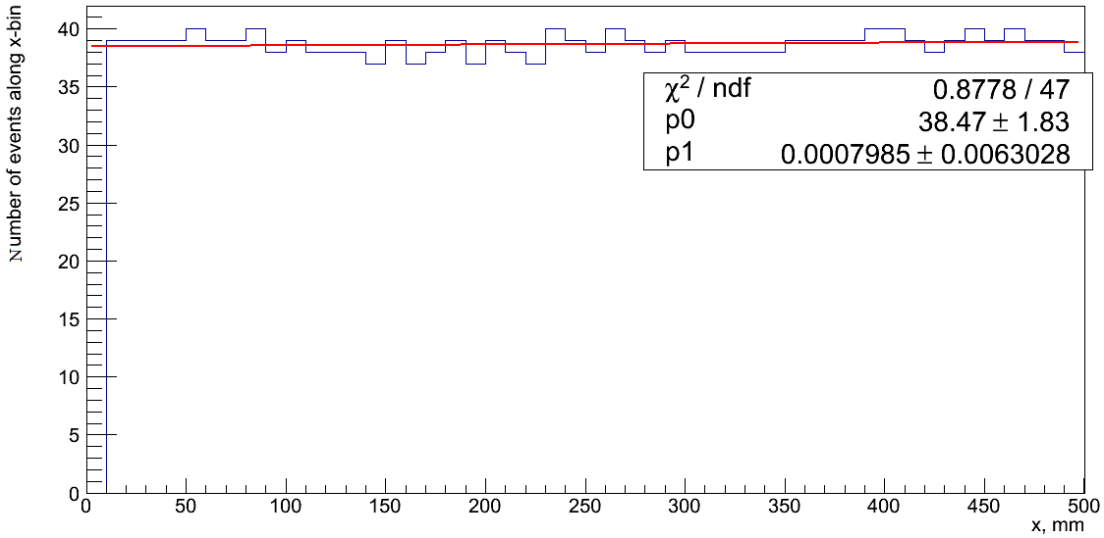

Figure 8: Distribution of initial *x*-coordinate of progenitor particles

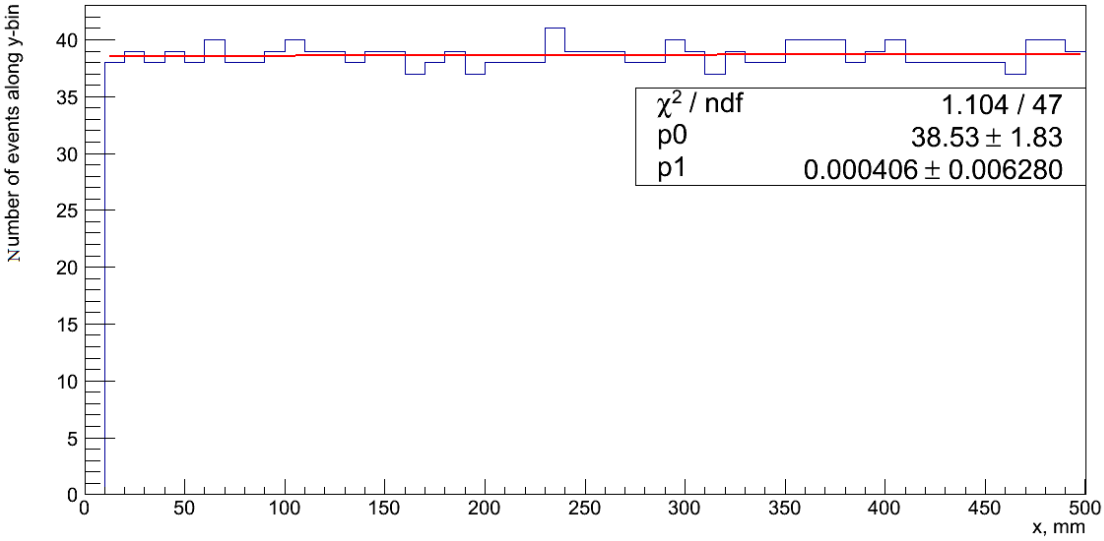

Figure 9: Distribution of initial y-coordinate of progenitor particles

7.2. Zenith angle

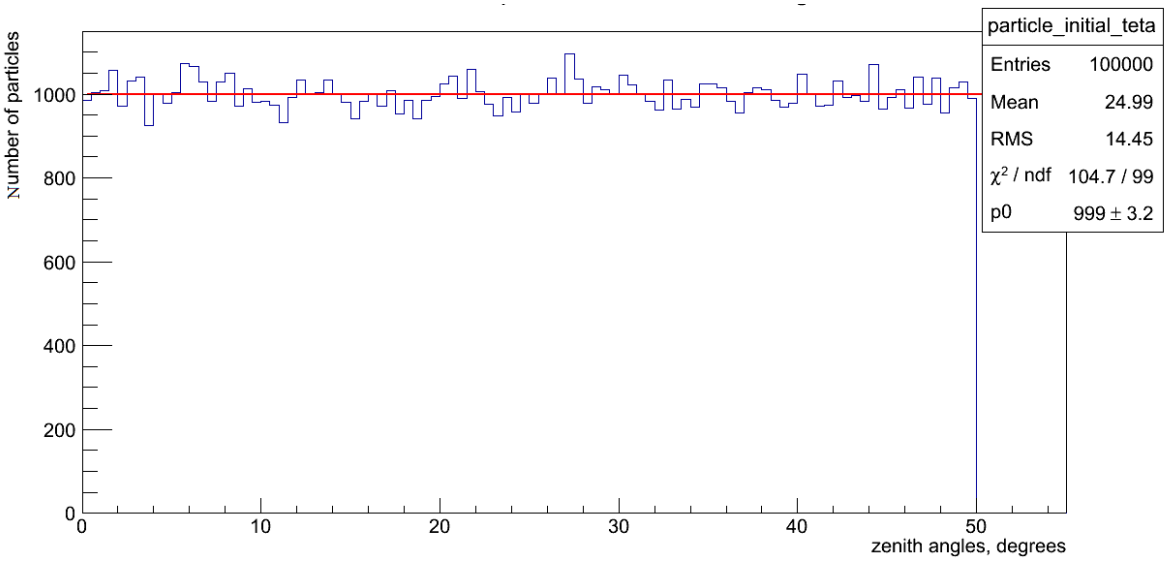

Figure 10: Distribution of initial zenith angle θ of progenitor particles

The same test as in the previous section has been done with initial zenith angle distribution of progenitor particles. According to the result presented in

Figure 10, zenith angle distribution is uniform as well. Note that the distribution has been fitted with constant function instead of linear function.

7.3. Light yield isotropy

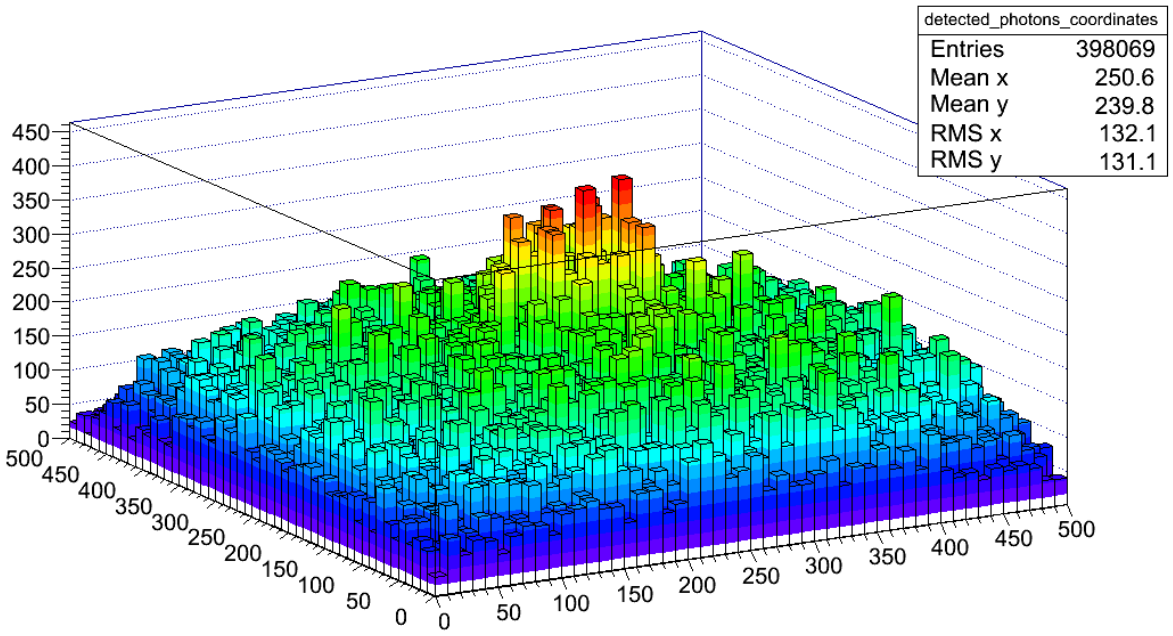

Figure 11: Distribution of detected photons' progenitor particles' initial *x,y*-coordinates for scintillator detector with PMT above

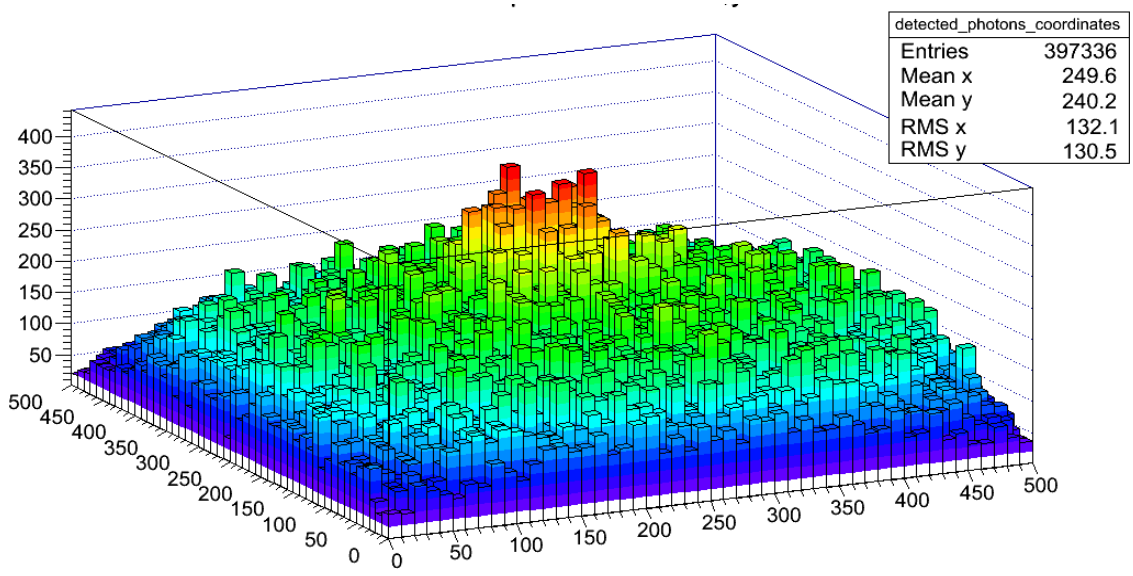

Figure 12: Distribution of detected photons' progenitor particles' initial *x,y*-coordinates for scintillator detector with PMT below

As mentioned above, scintillator gives an isotropic light yield. Whether simulation gives the same feature (that is, to check if the implemented physics is correct) has also been checked separately. Result for detector with PMT above is in

Figure 11, with PMT below is in Figure 12. Note that both arrangements are symmetric, that is, if PMT is above the scintillator then the bottom side is painted white, whereas if PMT is below, the top side is painted white. Also, note that the number of emitted photons per step used for this test is less than in experimental data. It has been done to decrease the time of simulation run.

Note from Figures 9 and 10 that the light yield for both distributions is almost the same, although geometry with 'PMT above' results in a slightly higher light yield within statistical deviation: 398069 detected photons for detector with 'PMT above', 397336 photons for 'PMT below'. When compared, Kolmogorov-Smirnov test gives 0.99 probability that these histograms are similar. It can be concluded that both histograms are same, that is, the simulation of scintillator detector indeed gives isotropic light yield.

7.4. Light yield vs. zenith angle θ

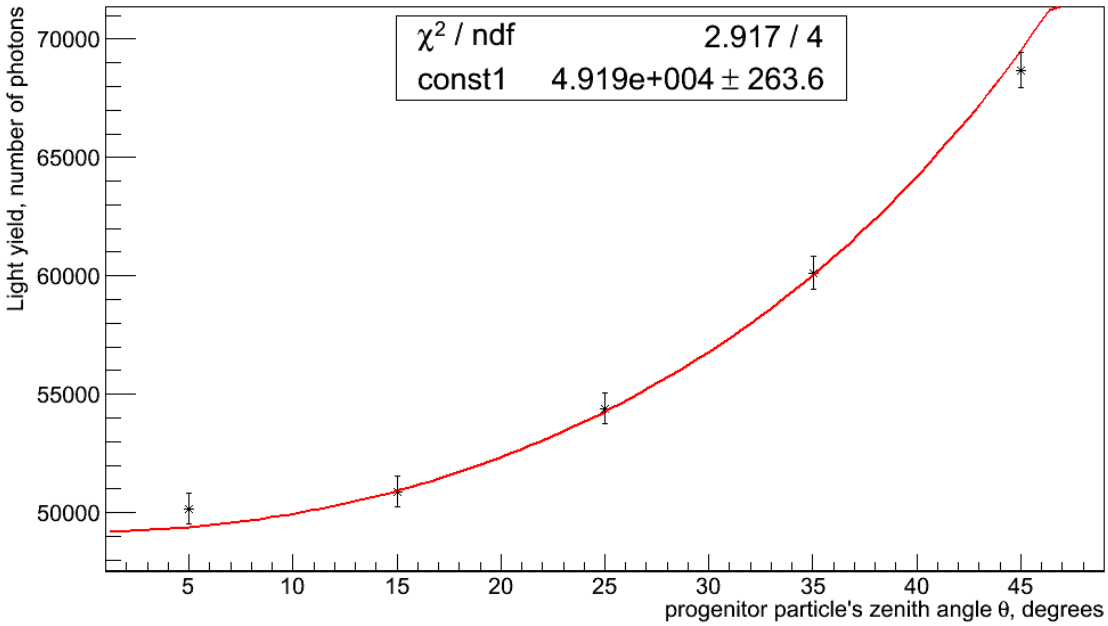

Figure 13: Scintillator detector light yield vs progenitor particles' zenith angle

It is expected that the scintillator light yield increases proportionally to $\frac{1}{\cos\theta}$, where θ - progenitor particles' zenith angle. Simulation results for particles passing at different θ are presented in Figure 13. The data is fitted with function:

$$y = \frac{const1}{\cos\theta} \qquad (12)$$

Parameter *const1* in Eq. 12 is for scaling and can be extracted from the data, although it does not play any crucial role. As it can be seen, light yield for scintillator coincides with expectation, since data fits with Eq. 12 very good.

7.5. Signal width vs. zenith angle θ

An example of the detected photons time arrival distribution obtained from the simulation run for angles interval $[\frac{\pi}{6}; \frac{2\pi}{9}]$ is in Figure 14. This distribution is taken as a PMT response signal for all simulation output data. The distribution can be fitted by Eq. 13:

$$f(t) = \int_0^\infty p(t')g(t-t')dt' \qquad (13)$$

where $p(t')$ - photon propagation function, which depends on atomic properties of the detector's materials, $g(t) = \frac{1}{\sqrt{2\pi}\sigma} e^{-\frac{t^2}{2\sigma^2}}$.

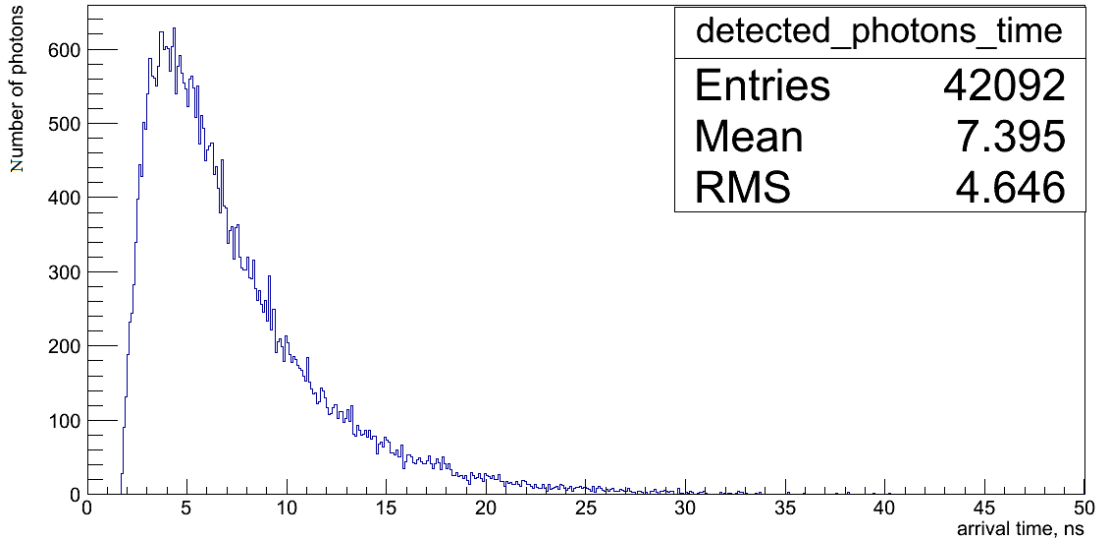

Figure 14: Example of detected photons arrival time distribution

Signal width in this simulation is defined as a full width at half-maximum of the distribution of detected photons' arrival time. It is expected that the signal width of scintillator detector remains constant for all values of θ due to isotropy of the scintillation light. Simulation results presented in Figure 15 coincides with this expectation (error bars are very small).

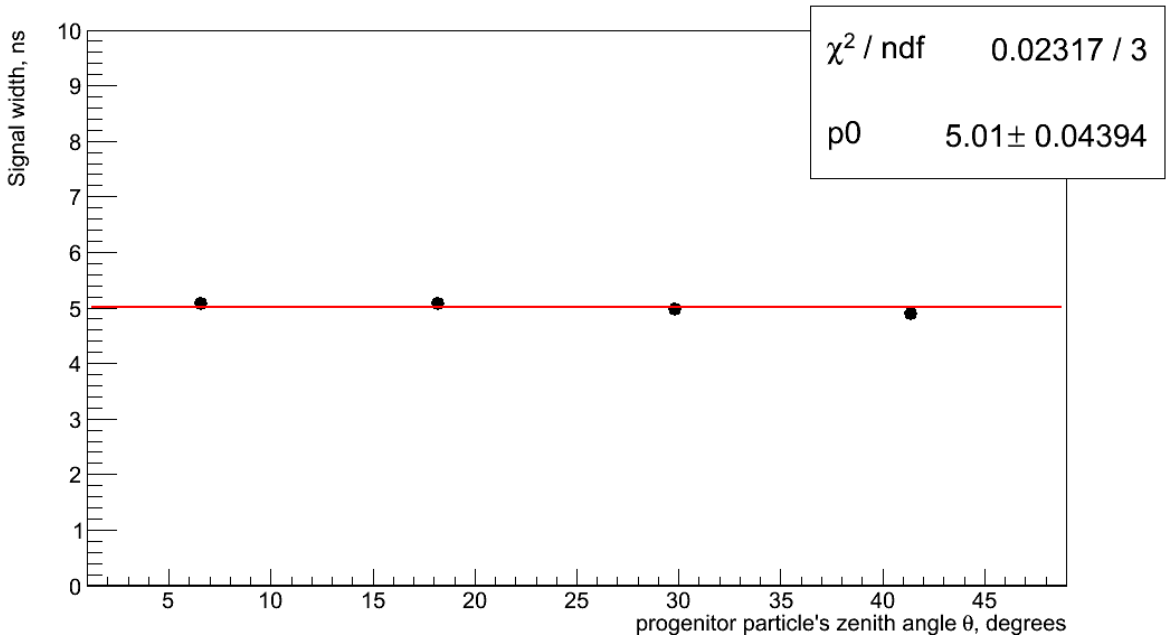

Figure 15: Scintillator signal width yield vs progenitor particles' zenith angle

7.6. Uniformity vs. zenith angle θ

There is no rigorous definition of how to determine the uniformity of the detector. For this simulation activities the following procedure has been used [14]:

1. dividing histogram of spatial distribution of detected photons by histogram of spatial distribution of progenitor particles;
2. taking number of detected photons per particle (obtained distribution corresponds to this data) along 8 separate lines: both diagonals, x = 150, 250, 350, y = 150, 250, 350mm;
3. normalizing all 8 1D-histograms such that maximum of each histogram is equal to 1;
4. calculating mean and standard deviation for each histogram;
5. compute uniformity coefficient as a mean of all 8 means calculated previously with the corresponding standard deviation.

The closer to 1 the uniformity coefficient value is, the more uniform the detector arrangement is. This coefficient is expected to remain constant for all values of θ. Simulation results in **Error! Reference source not found.** coincide with this claim.

Note that the large error bars, that is, large standard deviations of the data can be explained by examining Figure 12, where 2D distribution of detected photons' initial coordinates is shown. It is easily seen that the distribution of the detected photons is not uniform, but this distribution is linearized to compute the uniformity coefficient. Such procedure results in large standard deviations.

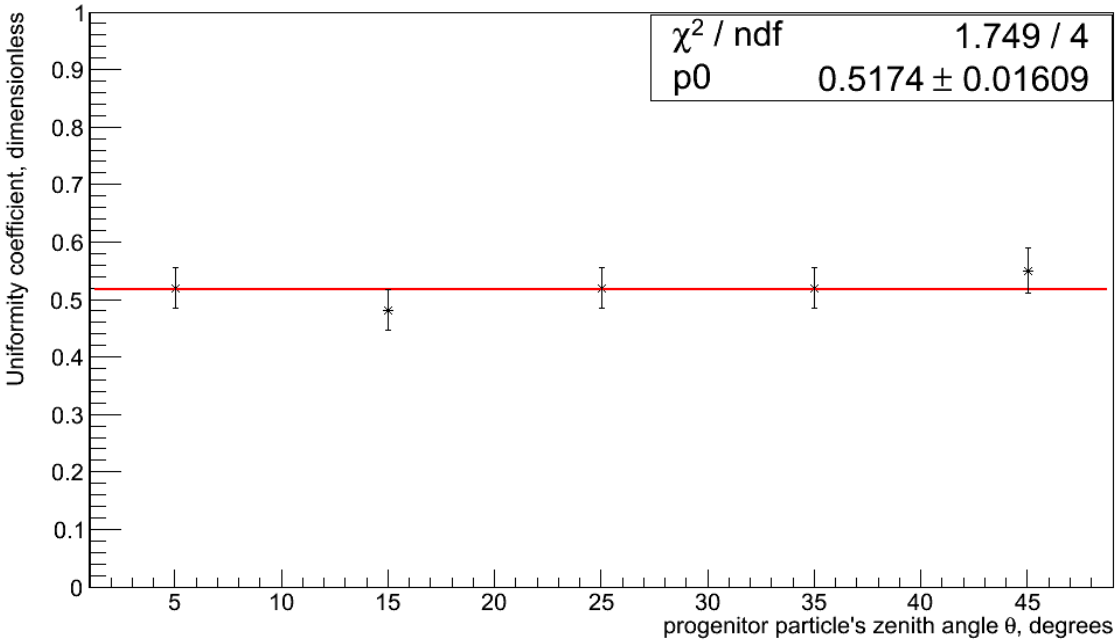

Figure 16: Scintillator uniformity coefficient yield vs progenitor particles' zenith angle

Also, note that the values in **Error! Reference source not found.** correspond to the small sample of progenitor particles. The uniformity coefficient for the tested scintillator detector arrangement obtained experimentally is equal to 0.7±0.06, and the simulation with bigger sample of particles gives a value of 0.70±0.04, which coincides with the experiment. Such dependence on the sample size does not affect expected simulation results, since statistical behavior remains the same regardless of the sample size and the bigger samples are used for the main simulation activities described in the next section.

8. Glass detector simulation

After successful check of simulation validity using scintillator detector model, a glass option for detection medium that has been tested, its physics implemented in simulation is described above. First, glass detector isotropy is checked. According to the results, arrangement with PMT above results in more efficient light detection. Then, dependence on θ of 3 parameters of the chosen glass detector geometry are tested: light yield, signal width and uniformity coefficient. A sample of 10^5 particles is used for isotropy check, a sample of $5 * 10^4$ is used to study parameters of the chosen geometry at simulation runs. One of the issues for this model is that its performance has not been investigated before. Thus, all of the results presented below are simulation-based only and still need experimental confirmation.

8.1. Isotropy

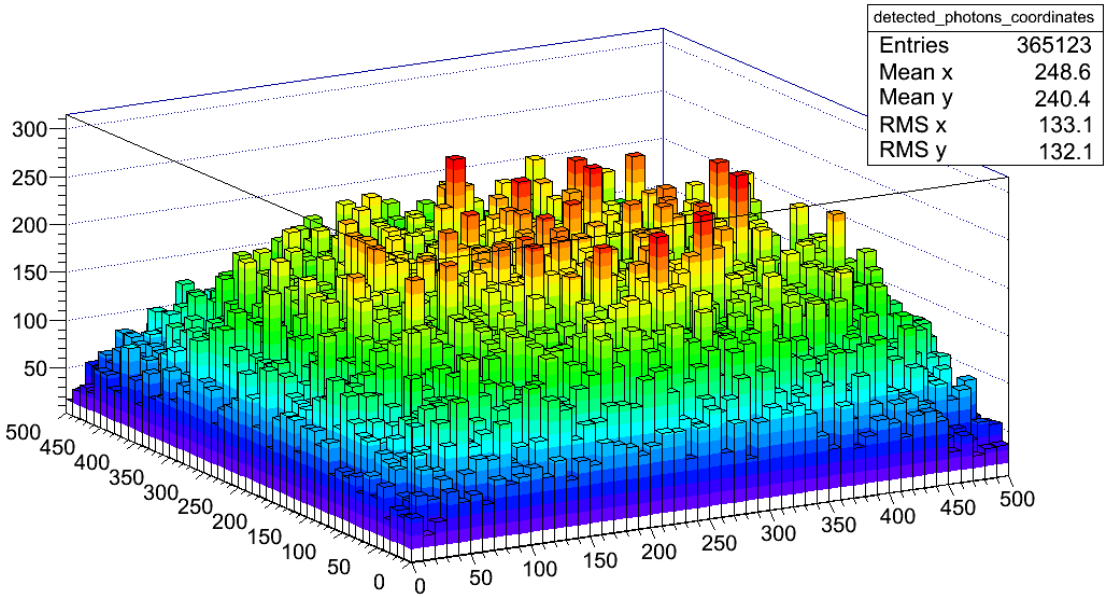

Figure 17: Distribution of detected photons' progenitor particles' initial x,y-coordinates for glass detector with PMT above

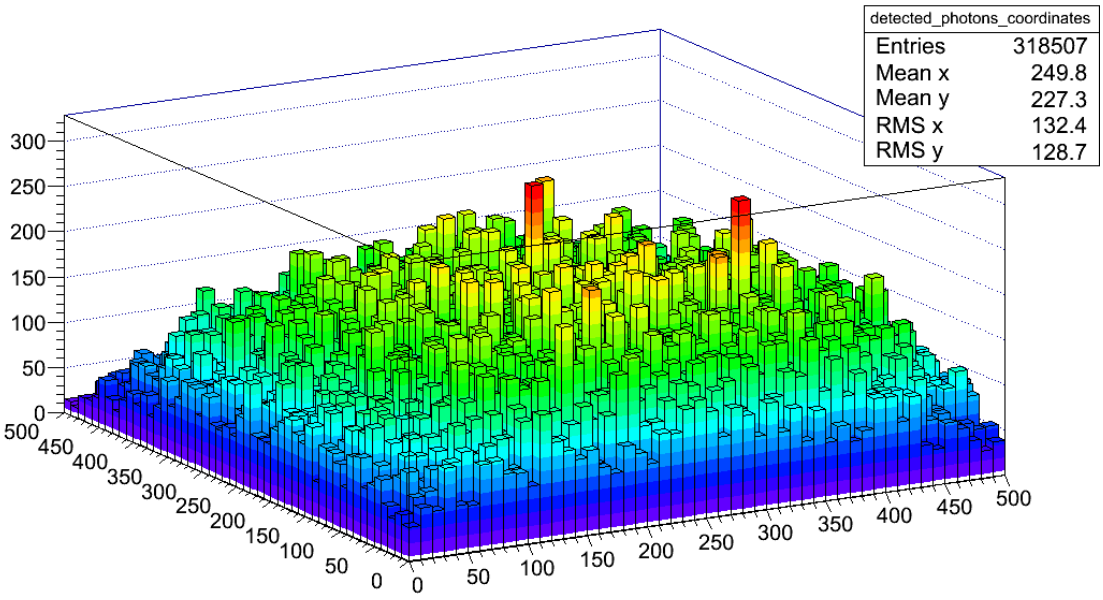

Figure 18: Distribution of detected photons' progenitor particles' initial *x,y*-coordinates for glass detector with PMT below

Simulation results for the arrangement with PMT above is in **Figure** 17, with PMT below - in Figure 18. From these Figures is can be seen that the first geometry results in a significantly larger number of detected photons (365123 detected photons vs. 318507), so it is a more efficient arrangement for light detection. Kolmogorov-Smirnov test gives 0.001 similarity probability. It indicates that there is no isotropy in glass detector as expected. Thus, the arrangement with PMT above has been chosen for further simulation tests of glass detector. Note that both geometries are similar to scintillator detector ones in terms of PMT placement and painting of detection medium, as described in section 7.3.

8.2. Light yield vs. zenith angle θ

Simulation results for glass detector light yield dependence on θ are shown in Figure 19. Note that the data distribution has a clear maximum and a minimum, although variations are not large, light yield varies between ~35000 and ~39000 detected photons. Existence of minimum and maximum can be explained by the fact that the emitted Cherenkov light is not isotropic and is distributed in a cone, and this physics results in such a behavior of glass detector performance, but this feature still needs experimental investigation.

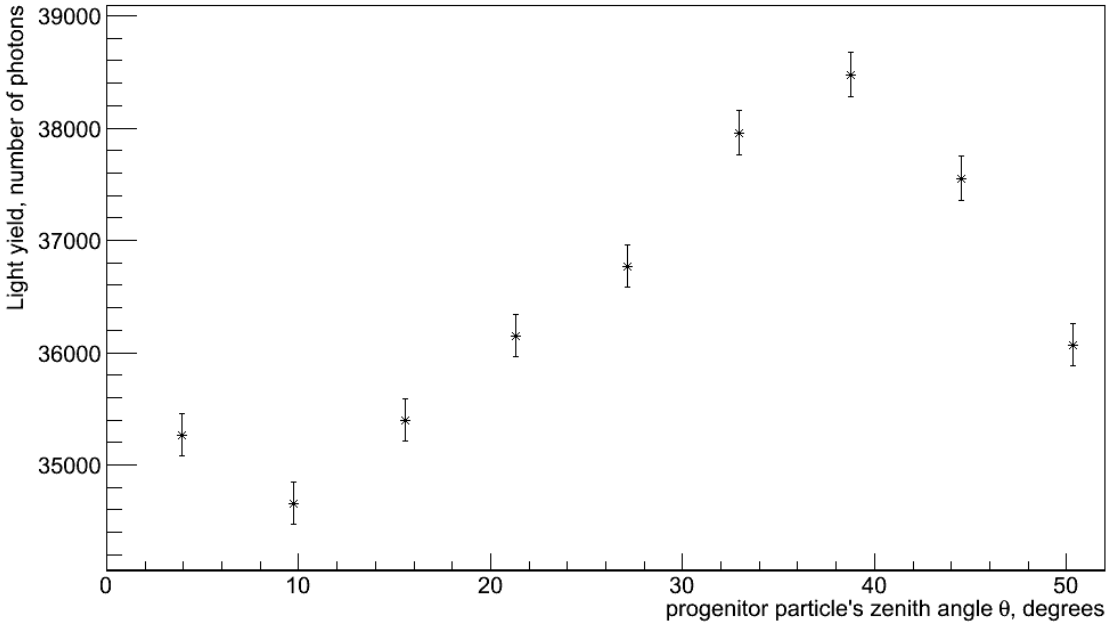

Figure 19: Glass detector light yield vs progenitor particles' zenith angle

8.3. Signal width vs. zenith angle θ

Simulation results for the dependence of glass detector signal width on θ are in Figure 20. The distribution is fitted with a linear function. Note that the signal width does not remain constant as with the corresponding results for scintillator detector, but gradually increases. This feature again can be explained by the physics of the Cherenkov radiation in glass, but needs experimental investigation as well.

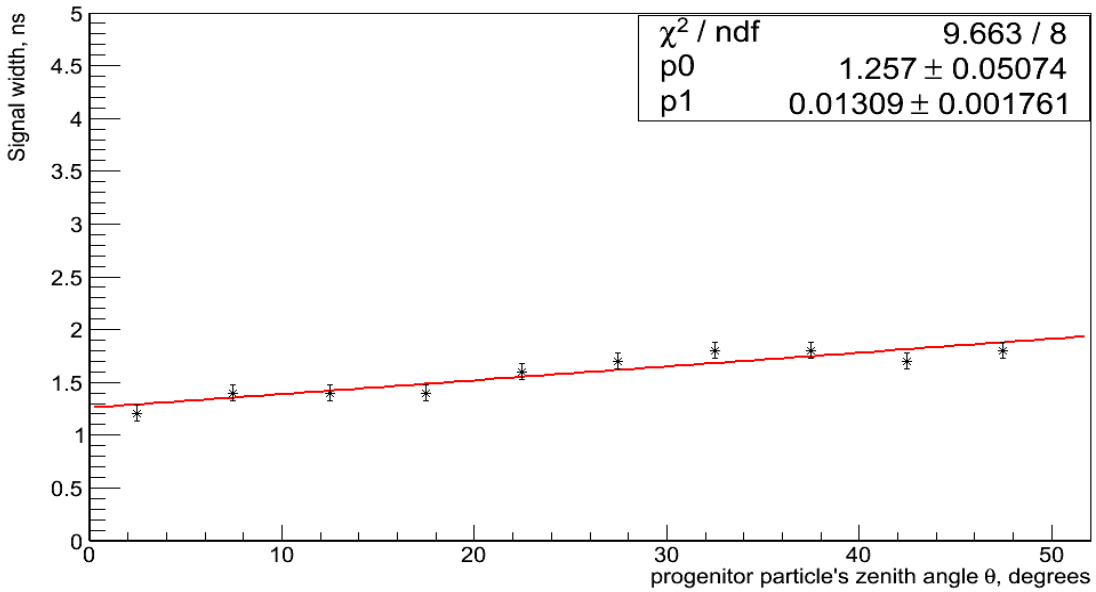

Figure 20: Glass detector signal width vs progenitor particles' zenith angle

8.4. Uniformity vs. zenith angle θ

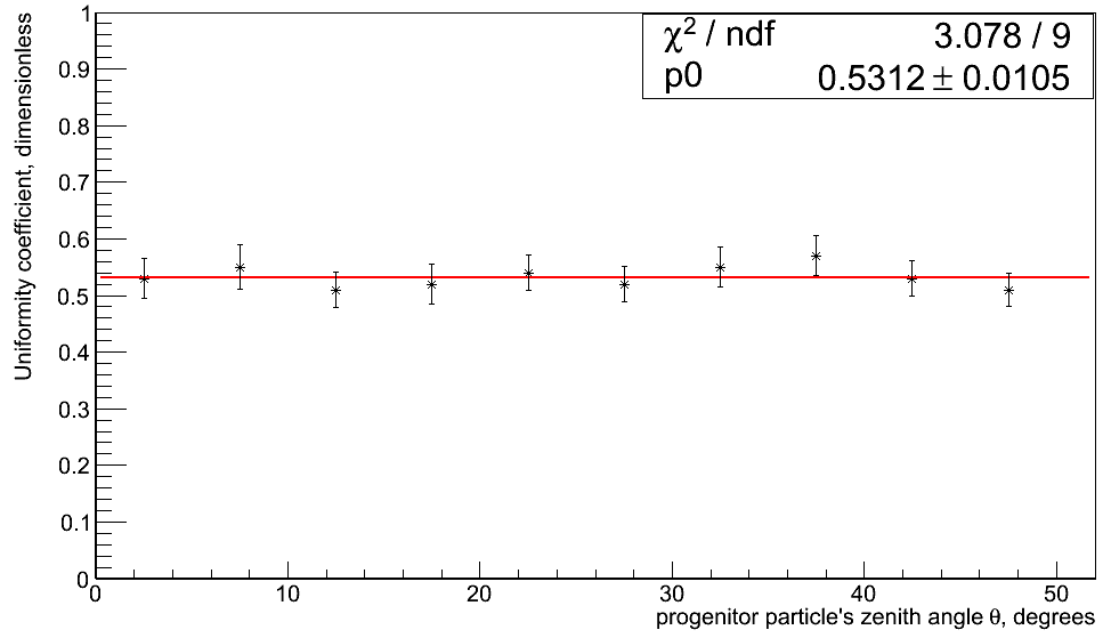

Figure 21: Glass detector uniformity coefficient vs progenitor particles' zenith angle

Simulation results for the dependence of glass detector uniformity coefficient on θ are in

Figure 21. The data is fitted with constant function. Note that these results are similar to that of scintillator since no large variations are observed. The data values correspond to the smaller sample size, using bigger sample results in the value of uniformity coefficient equal to 0.77±0.06. [22]

8.5. Discussion

According to the results presented in this section, some interesting features of glass detector performance have been observed. The manner, in which this material responds to the

different inclinations of incoming particles' trajectory, needs future experimental studies. In addition, a phenomenon of signal width increase needs the same investigation. For now, it can be claimed that the glass detector has better uniformity than the scintillator one does. However, light yield is significantly higher for the scintillator as known. These differences will be more notable in the next section, where 4 different geometries will be compared: two for glass and two for scintillator.

9. Comparison of 4 detector models

In this section simulation results for 4 different detector arrangements are presented. These arrangements are glass detector with white sides ("white glass"), glass detector with black sides ("black glass"), scintillator detector with white sides ("white scint"), scintillator detector with black sides ("black scint"). In all of the simulated models PMT is placed above the detection medium at distance equal to the detection medium base side, value of the amount of the emitted photons per propagation step is set to correspond to the real data (~40 photons/mm for glass, ~560 photons/mm for scintillator for a total of ~18.5 photons per MIP). A sample of 10^5 particles is used. The purpose of the comparison of these 4 arrangements is to determine whether detector's lateral sides should be painted black or white and to check how well each model performs. Light yield, signal width and uniformity coefficient are taken again as the parameters for the comparison, their values are in Table 1.

Table 1: Parameters of 4 geometries obtained from the simulation

Medium Type	Light Yield, number of detected photons	Average signal width, ns	Uniformity
Black Glass	181062±426	1.8±0.1	0.74±0.03
White Glass	230610±480	2.1±0.1	0.77±0.02
Black Scint	1609049±1269	7.5±0.1	0.68±0.04
White Scint	1892122±1376	9.2±0.1	0.70±0.04

9.1. Light yield

The standard errors for the values are square root of the value themselves, because the photon emission is Poisson distribution. Note a large difference between light yields for the scintillator and for the glass. It can be easily explained by the fact that the amount of emitted photons/mm is ~16 times bigger for the scintillator than for the glass. Note that the models with white sides give bigger light yield than the models with the same detection medium, but with black sides. Such behavior is expected, because black color absorbs more light than white color does. As a result, more photons reach PMT region for the models with white lateral sides.

9.2. Signal width

In this case the standard deviations are sums in quadrature of width of two histogram bins, because the uncertainties in FWHM exist from both right and left sides. Note that the signal width values are averaged over all angles. The scintillator models give wider signals than glass models, it can be explained by the fact that the optical rise time of the glass medium is notably less than that of the typical scintillator. In the simulation, these values are 100ps for glass and

4.5ns for scintillator. Also note that the signal width for the models with white sides is bigger than for the models with black sides. When emitted photons experience a lot of reflections from lateral sides, their propagation path increases. According to Eq. 7, total travel time increases as well, and, since distribution of the detected photons arrival time is taken as a response signal of PMT, the signal width increases correspondingly.

9.3. Uniformity

The values for scintillator models are less than for the glass. Note than the highest uniformity coefficient (0.77±0.02) is obtained for the "white glass" model, the lowest one (0.68±0.04) is for the "black scint" model. Values for arrangements with white sides are again larger. It can be explained by the fact that the white lateral sides allow more photons emitted farther away from the detector center to reach and to be detected by PMT, what increases the value of the uniformity coefficient for these models. Although the difference between scintillator and glass detectors can be easily noticed, one should take into account that the values are obtained with large errors (this feature has been discussed in the section 7.6).

9.4. Discussion

From the results presented in this section we can suggest that the detectors with white lateral sides perform better than the ones with black sides, because these models give better light yield and uniformity, although values of signal width for models with black sides are less. However, it is still hard to rigorously determine which detection medium should be chosen for implementation, because, although the glass gives much less light yield than the scintillator, its uniformity coefficient is higher. Experimental investigations will help to determine which material should be used for detector construction, their results may either confirm or disprove the simulation results.

10. Conclusion

Results of the detector module simulation for the HT-KZ cosmic ray detector system have been presented in this paper, these results are to be used for the construction of the whole system. First, a phenomenon of EAS is briefly considered. Then HT-KZ system and its predecessor, HT system located at TSHASS, are overviewed, their main operating principles and implemented technologies are described. According to the results, regardless of the choice for the detection medium, the detector lateral sides should be painted white, because it helps to get better light yield and uniformity, although width of the signals from such detector increases due to an increase in a light pathlength. However, simulation did not show an optimal choice for the detection medium, because results for both scintillator and glass have their own pros and cons: scintillator has higher light yield, glass has better uniformity.

11. Future plans for HT-KZ development

As it has been mentioned, the simulation results are mainly used for HT-KZ system design and construction. Although a lot of work have been done so far, there is more work to do including additional simulation activities and experimental studies. A short list of future plans for HT-KZ construction and installation is below.

- Detector R&D finishing:
    - Attempting other options for detection medium;
    - Testing other possible geometries and PMT placements (check for the rise time and signal width);
- Pulse synchronization R&D:
    - improvements in the DAQ software;
- Construction of detection units and their installation on the rooftops of NU;
- Collecting first data and comparing with the existing results from HT and other similar detection systems.

Bibliography

[1] P. L. Biermann, J. K. Becker, L. Caramete, A. Curutiu, R. Engel, H. Falcke, L. A. Gergely, P. G. Isar, I. C. Maris, A. Meli, K.-H. Kampert, T. Stanev, O. Tascau, C. Zier, "Active Galactic Nuclei: Sources for ultra high energy cosmic rays?," *arXiv:0811.1848 [astro-ph]*, 2009.

[2] P. Blasi, R. Dick, E.W. Kolb, "Ultra-high energy cosmic rays from annihilation of superheavy dark matter," *arXiv:astro-ph/0105232,* 2002.

[3] B. Rossi, "Method of Registering Multiple Simultaneous Impulses of Several Geiger's Counters," *Nature*, no. 125, p. 636, 26 April 1930.

[4] P. Auger, P. Ehrenfest, R. Maze, J. Daudin, R. A. Fréon, "Extensive Cosmic-Ray Showers," *Rev. Mod. Phys.*, vol. 11, p. 288, 1 July 1939.

[5] M.T. Dova, "Ultra-High Energy Cosmic Rays," *arXiv:1604.07584 [astro-ph.HE]*, 2013.

[6] K.A. Olive et al. (Particle Data Group), "The Review of Particle Physics," *Chin. Phys. C*, 38, 090001 (2014).

[7] R.U. Beisembaev, E.A. Beisembaeva, O.D. Dalkarov, V.A. Ryabov, A.V. Stepanov, N.G. Vildanov, M.I. Vildanova, V.V. Zhukov, K.A. Baigarin, D. Beznosko, T.X. Sadykov, N.S Suleymenov, "The "Horizon-T" Experiment: Extensive Air Showers Detection," *arXiv:1605.05179 [physics.ins-det]*, May 17 2016.

[8] R.U. Beisembaev, V.P. Pavluchenko, A.V. Stepanov, G.S. Takibaev, "Muons of extra high energy horizontal EAS in geomagnetic field and nucleonic astronomy," *Proc. 24 ICRC. Roma. 1. pp 646-649*, 1995.

[9] D. Beznosko, A. Batyrkhanov, T. Beremkulov, A. Duspayev, A. Iakovlev, Z. Makhataeva, K. Yelshibekov, M. Yessenov, "Horizon-T extensive air showers detector system operations and performance," *in proceedings to ICHEP-2016 conference PoS(ICHEP2016)784*, 2016.

[10] D. Heck, G. Schatz, T. Thouw, J. Knapp, J.N. Capdevielle, "CORSIKA: A Monte Carlo code to simulate extensive air showers," *Forschungszentrum Karlsruhe Report FZKA (6019).*

[11] R. U. Beisembaev, "Detector system project for studies of EAS at energies above 10^17 eV," *AS News, KZ Rep, phys-math series, #6 C.*, pp. 74-76, 1991.

[12] R.U. Beisembaev et al., "The first results obtained with the HORIZON-T detector system," *Journal of Physics. 409. 012127.*, 2013.

[13] A. Duspayev, A. Batyrkhanov, T. Beremkulov, D. Beznosko, A. Iakovlev, M. Yessenov, "The distributed particle detectors and data acquisition modules for Extensive Air Shower measurements at "HT-KZ" experiment," *in proceedings to PhotoDet2015 conference*

PoS(PhotoDet20 1 55)06, 2015.

[14] A. Duspayev, R.U. Beisembaev, T. Beremkulov, D. Beznosko, A. Iakovlev, K. Yelshibekov, M. Yessenov, V. Zhukov, "Simulation, design and testing of the HT-KZ Ultra-high energy cosmic rays detector system," *Proceedings of ICHEP2016,* vol. PoS(ICHEP2016)721, 2016.

[15] J.V. Jelly, W.J. Whitehouse, "Proc. Phys. Soc. (London) A66 454," 1953.

[16] L.J. Bignell, D. Beznosko, M.V. Diwan, S. Hans, D.E. Jaffe, S. Kettell, R. Rosero, H.W. Themann, B. Viren, E. Worcester, "Characterization and modeling of a Water-based Liquid Scintillator," *Journal of Instrumentation, Vol. 10, p 12009, IOP Publishing,* 2015.

[17] "Hamamasu Photonics K.K., Electron Tube Division, 314-5, Shimokanzo, Iwata City, Shizuoka Pref., 438-0193, Japan," [Online]. Available: http://www.hamamatsu.com.

[18] "CAEN S.p.A. Via della Vetraia, 11, 55049 Viareggio Lucca, Italy.," [Online]. Available: http://caen.it.

[19] I.M. Sobol, The Monte-Carlo methods, Moscow: "Nauka", 1973.

[20] "Modeling Diffuse Reflection (or How to Sample Cosine Distribution)," 2 April 2015. [Online]. Available: https://www.particleincell.com/2015/cosine-distribution/.

[21] Beznosko, D; Beremkulov, T; Iakovlev, A; Makhataeva, Z.; Vildanova, M. I.; Yelshibekov, K; Zhukov, V. V., "Horizon-T Experiment Calibrations-Cables," *arXiv:1608.04312,* 2016/8/15.

[22] A. Duspayev, M. Yessenov, D. Beznosko, A. Iakovlev, M.I. Vildanova, V.V. Zhukov, "Glass-based charged particle detector performance for Horizon-T EAS detector system," *arXiv:1703.07919,* 2017.

[23] R.U. Beisembaev, "Lecture series on UHECR," *Tien Shan high-altitude cosmic station,* 2014-2017.